EFDA–JET–PR(10)45

M. Gelfusa, A. Murari, P. Gaudio, A. Boboc, D. Mazon, F. Avino, O. Tudisco
and JET EFDA contributors

New Approximations and Calibration Methods to Provide Routine Real Time Polarimetry on JET

New Approximations and Calibration Methods to Provide Routine Real Time Polarimetry on JET

M. Gelfusa[1], A. Murari[2], P. Gaudio[1], A. Boboc[3], D. Mazon[4], F. Avino[5], O. Tudisco[5]
and JET EFDA contributors*

JET-EFDA, Culham Science Centre, OX14 3DB, Abingdon, UK

[1]Associazione EURATOM-ENEA - University of Rome "Tor Vergata" , Roma, Italy
[2]Consorzio RFX Associazione EURATOM-ENEA per la Fusione, 4-35127 Padova, Italy
[3]EURATOM-CCFE Fusion Association, Culham Science Centre, OX14 3DB, Abingdon, OXON, UK
4Association EURATOM-CEA, CEA Cadarache, 13108 Saint-Paul-lez-Durance, France
[5]Associazione EURATOM-ENEA – CR Frascati 00044 Frascati, Italy
** See annex of F. Romanelli et al, "Overview of JET Results",*
(23rd IAEA Fusion Energy Conference, Daejon, Republic of Korea (2010)).

Preprint of Paper to be submitted for publication in
Plasma Physics and Controlled Fusion

ABSTRACT

The increasing importance of providing reliable polarimetric measurements in real time, for both machine protection and plasma control, has motivated the development of a quick version of the calibration algorithms for JET polarimeter. This new code, which interprets the calibration procedure performed before each shot, is based on a physical equivalent model of the diagnostic optical path and is valid for any operational regime of JET. It provides results before the plasma breakdown and, with its calibration constants, the polarimetric measurements have an accuracy more than sufficient for real time purposes. New approximate equations have been validated to obtain the line integrated density from the horizontal chords, so that also these polarimetric measurements can also be used for density feedback and machine protection. The availability of reliable polarimetric measurements in real time opens new perspectives also to the determination of the plasma boundary and the magnetic equilibrium and their use in feedback control.

1. INTRODUCTION

The importance of providing reliable measurements in real time for control of Tokamak plasmas has become increasingly evident in the last years. The operation of the next generation of devices, such as JET with a metallic wall and ITER, will impose even more stringent requirements on the diagnostics for real time. More quantities will have to be provided with higher accuracy and more reliably. The use of these measurements range from simple Single Input Single Output (SISO) schemes for machine protection to more involved Multiple Inputs Multiple Outputs (MIMO) systems for sophisticated control of advance plasma experiments (see section 8).

One of the diagnostics whose data in real time would really open new perspectives to control is polarimetry. Thermonuclear plasmas are active and anisotropic media, which strongly affect the propagation of electromagnetic radiation, depending on their parameters. The measurement of the change in the polarization state (Faraday rotation and Cotton-Mouton effect) of a laser beam probing a plasma can therefore provide very useful information about various physical quantities crucial for both the understanding of the physics and the control of the configuration. The measurement of the Faraday rotation is one of the very few techniques to probe the magnetic fields inside a thermonuclear plasma. This information is therefore essential to obtain realistic equilibria [1]; these measurements have therefore been used extensively in the past for real time control of the magnetic configuration and of the q profile in particular [2]. Obtaining the line integrated density from the phase shift is also very appealing particularly for machine protection. Indeed interferometry, the reference measurement of the electron density in Tokamak, can be affected by fringe jumps. Once a fringe jump has occurred the interferometric measurement is compromised for the whole discharge and techniques to overcome the problem have not proved completely satisfactory so far [3]. Obtaining a reliable estimate of the line integrated density from polarimetry would alleviate this problem, since the Faraday rotation and phase shift are no affected by fringe jumps. The importance to provide reliably this quantity is significant for control, to implement machine protection schemes such as the protection of the wall

from shine through of the neutral beam when the density becomes too low.

On JET, a dual interferometer/polarimeter system performs, routinely, the Faraday rotation and Cotton-Mouton phase shift measurements. On JET these measurements are complicated by two facts: first the general issue of the nonlinear interaction between the Faraday rotation and the Cotton Mouton effect and second a "anomalous" phase shift induced by non identified optical components of the diagnostic. The effect of this anomalous instrumental phase shift must be taken into account in the calibration and signal processing procedures.

Since the optical components introducing the anomalous effects are completely unknown, the previous algorithms to interpret the calibration data were based on empirical models in which purely numerical and quite complex fitting procedures were implemented to evaluate the calibration parameters and the polarimetric measurements. This processing method was developed without any investigation on the source of the phase shift anomaly and it works as a black box without a clear relation with the hardware setup (for example these calibration procedures do not make any attempt to separate the electronics from the optical instrumental effects). A statistical analysis, carried out on the polarimetric measurements acquired during the campaigns 2003-2009, has highlighted some calibration problems affecting mainly the experimental data of the most recent campaigns (2008-2009), particularly those of the high current discharges. Therefore, it has been decided to develop a new calibration code, separating the electronics from the optical instrumental effects. The electronics calibration constants are determined independently (see section 2.3) and an independent algorithm models the optical layout of the diagnostic. This new approach resulted in a more transparent calibration code, with better performance in terms of accuracy; moreover the new algorithm is capable of properly modelling the behaviour of the diagnostic for all the various configurations, including the ones optimised for high current operation (see section 2 and references for more details). On the other hand, the original version of the new calibration algorithm was developed for offline analysis. Given the good results obtained and the increasing importance of obtaining sound polarimetric measurements in real time (for example to correct fringe jumps in the interferometer or to provide the q profile), it has been investigated the opportunity to develop a new version of the calibration algorithms to be run automatically before each discharge. Indeed between 14 and 18 s before the plasma breakdown, an automatic calibration procedure is run for each JET discharge. One of the subject of the present paper is therefore to describe new calibration algorithms to interpret the calibration data capable of providing reliable results in the interval between the end the calibration procedure and before the beginning of the plasma. For the vertical chords, these new calibration algorithms guarantee good measurements of the Faraday rotation, which can be used directly in equilibrium codes, and the phase shift which can immediately provide the line integrated density for any required purpose. On the other hand, for horizontal chords no formula was available to directly derive the line integrated density from the polarimetric measurements. New approximations have been found which guarantee a line integrated measurements or the horizontal chords within 1 fringe of the interferometric values ($1.14 \cdot 10^{19} \mathrm{m}^{-2}$).

With regard to the structure of the paper, in section 2 polarimetry and its implementation on JET is synthetically reviewed. The hardware calibration procedure and the new algorithm to derive the calibration parameters are presented in section 3. The version of the calibration algorithm that can be run in a short interval before any shot, to update the calibration constants on a shot to shot basis is presented in section 5. In section 6 the results obtained for the vertical chords are described in detail. The version of the calibration code for the horizontal chords is described in section 6 and in section 7 new approximate formulas to obtain the line integrated density from these lines of sight are discussed. The importance of reliably providing calibrated polarimetric measurements in real time is illustrated in section 8 by some recent examples, including the magnetic topology obtained with a new real time equilibrium code developed for JET. Conclusions are the subject of the last section 9 of the paper.

2. POLARIMETRY AND ITS IMPLEMENTATION ON JET

2.1 POLARIMETRIC MEASUREMENTS

Two separate phenomena influence the polarisation of a Far InfraRed (FIR) beam that passes through a magnetically confined plasma [4]:

- **Faraday Rotation effect:** the plane of linearly polarised light passing through a plasma is rotated of an angle $\Delta\Psi$ which depends on the magnetic field component parallel to the direction of propagation according to the relation

$$\Delta\Psi \propto \lambda^2 \int n_e \cdot B_{\parallel} \cdot dz \tag{1}$$

- **Cotton-Mouton effect:** the ellipticity Φ acquired by a linearly polarised light passing through a plasma is dependent on the density and the magnetic field perpendicular to the direction of propagation.

$$\Phi \propto \lambda^3 \int n_e \cdot B_{\perp}^2 \cdot dz \tag{2}$$

In equations (1) and (2) λ is the laser wavelength, n_e is the plasma electron density and $B_{\parallel}$ and $B_{\perp}$ the parallel and perpendicular components of the magnetic field respectively. After traversing the plasma a polarised beam suffers a rotation of the polarisation plane due to Faraday Rotation and acquires ellipticity due to the Cotton-Mouton effect.

2.2 BRIEF DESCRIPTION OF JET INTERFEROMETER/POLARIMETER

On JET, the FIR diagnostic operates as a dual interferometer/polarimeter [5, 6]. The system probes the plasma with 4 vertical and 4 lateral laser beams. The diagnostic provides of the line-integrated plasma density measurements by means of interferometry and Faraday Rotation angle and Cotton-Mouton phase shift measurements by polarimetry. The layout of the instrument is shown in figure 1

The main characteristics of the experimental set-up are:

- the diagnostic involves the use of far infrared lasers because this is a good compromise between the conflicting needs of increasing the sensitivity of the instrument and of avoiding the cut-off at the plasma frequency [7];
- two FIR lasers (195μm Deuterated Cyanide (DCN) and 119μm Methanol), modulated at two different frequencies, allow vibration induced and plasma induced phase shifts to be measured (in the past only the horizontal chords were equipped with the second colour for vibration compensation but for the next campaigns a second wavelength will be implemented also on the vertical chords);
- very long optical path: about 80 metres for each of its 8 channels;
- the time resolution of 10μs;

The Faraday rotation angle is measured on all 8 channels by evaluating the two components of polarisation of the laser beam that passes through the plasma. These measurements are preceded by an on-line calibration procedure performed before each shot (using half-wave plates) [5, 6]. In order to measure the Cotton-Mouton angle, a special set-up, with initial linear polarisation of the input beam set at 45 degrees with respect to the toroidal field direction (x-axis) for the vertical channels and parallel to the toroidal field for the horizontal channels, has been implemented.

The schematic of the polarimetry at JET for one vertical chord is shown in figure 2.

The Half-Wave Plate (HWP1) at the entrance window is used to set the required direction of the linear input polarisation. During the calibration, this half-wave plate is rotated before each discharge to simulate the Faraday rotation effect (see section 3).

The amplitudes of the measured beat signals are proportional to the orthogonal components of the corresponding electric field vector amplitudes of the electromagnetic wave in the local co-ordinate system [6] defined by the orientation of the wire grid in front of the detectors:

$$p(t) \propto E_y \cos(\omega_0 t - \varphi) = E_y^0 \sin\Theta \cdot \cos(\omega_0 t - \varphi) \tag{3}$$

$$i(t) \propto E_x \cos(\omega_0 t - \varphi) = E_x^0 \sin\Theta \cdot \cos(\omega_0 t) \tag{4}$$

where ω_0 is the modulation frequency (100kHz) obtained by a rotating grating wheel, φ is the phase shift between the orthogonal components, E_x and E_y are the components of the electrical vector, and $\Theta = \Theta_0 + \alpha$ with $\Theta_0 = 45^o$. In presence of plasma α represents the Faraday angle.

The amplified signals are sent to a phase sensitive electronic module to produce four additional signals that are sent to the data acquisition system.

2.3. SIGNAL PROCESSING ELECTRONICS

The signals detected by the two detectors (called i(t) and p(t)) are processed via analog phase sensitive electronics to obtain the following measurements: RMS, RMP, PSP and PSD as shown in figure 2 :

$$RMS = \langle i(t) \times i(t) \rangle \tag{5}$$

$$RMP = \langle i'(t) \times i'(t) \rangle \tag{6}$$

$$PSD = \langle i(t) \times p(t) \rangle \tag{7}$$

$$PSP = \langle i' (t) \times p(t) \rangle \tag{8}$$

where $\langle i' (t) \propto \sin (\omega_0 t) \rangle$ is generated by shifting of 90 degrees the phase of the i(t) signal.
These four signals are processed by a code to obtain the two ratios R and R' which are related to the polarimetric parameters of the radiation coming out from the plasma:

$$R = \frac{PSD}{RMS} = C^{-1} \tan (\Theta) \cdot \cos \varphi \tag{9}$$

$$R = \frac{PSP}{\sqrt{RMS \cdot RMP}} = C^{-1} \tan (\Theta) \cdot \sin \varphi \tag{10}$$

where C is a calibration factor, given by the ratio $E_x^{\,0} / E_y^{\,0}$.
The main parameters of the electrical vector of the polarised radiation can be derived from R and R' using the following relations:

- the phase shift

$$\varphi = \text{arctg} \frac{R'}{R} = \phi_0 + \Phi \tag{11}$$

where ϕ_0 is the phase shift between the two signals in absence of plasma, while Θ represents the angle introduced by the Cotton- Mouton effect.

- the ratio Θ between the orthogonal components of the electrical vector

$$R^2 + R'^2 = C^{-2} \tan^2 \Theta \Rightarrow \tan^2 Q = C^2 (R^2 + R'^2) \tag{12}$$

The optical properties of the polarised light, polarisation angle (ψ) and ellipticity ($\varepsilon = \tan \chi$) can be derived using the well known identities, which relate the electrical parameters to the geometrical ones:

$$\tan (2\psi) = \tan (2\Theta) \cos \varphi \tag{13}$$

$$\sin (2\chi) = \sin (2\Theta) \cos \varphi \tag{14}$$

The parameter ψ is the polarisation angle between the major axis of the polarisation ellipse (see figure 3) and the reference x-axis; the parameter χ is related to the ellipticity of the radiation.

The present electronics used to process the signals from the detectors of the JET FIR polarimeter has been commissioned in 2002. Since in the last years the diagnostic has been configured for measuring routinely both the Faraday Rotation effect and the Cotton-Mouton effect with a different optical set-up, it was important to check the performance of the analog phase sensitive electronics [6]. To this end, the main operations performed by the analog electronics of the polarimeter have been implemented via software using both Simulink and Matlab [8]. This has allowed an accurate characterisation of the instrument and an assessment of the quality of the provided measurements (calibration, performance, etc).

3. THE CALIBRATION PROCEDURE AND THE ALGORITHM TO DERIVE THE CALIBRATION CONSTANTS

3.1 THE CALIBRATION PROCEDURE

At JET an on-line calibration, to link the output voltage of the detectors to the effective Faraday rotation angle and the phase shift, is carried out, for each chord, before each shot.

Currently, the procedure of calibration is the following: the half-wave plate, located at the entrance of the vacuum vessel (see fig.2), is rotated (via a step-motor) of a well-known angle and the phase shift is recorded at each angle, while the Faraday rotation is equal to twice the half-wave plate angle. This operation takes place in the interval between 18 and 14s before the plasma. These 14s are therefore the time allowed to run the calibration code and produce the required calibration parameters.

Moreover, before each campaign, or when it is necessary, a manual calibration is performed. It consists not only of the same steps, as the ones performed before the shots, but also of the fine tuning of the wire grid position, located in front of the two detectors. This allows modifying the repartition of the signal between the interferometric and the polarimetric detectors and therefore permits to optimise the setup of the diagnostic for the requirements of the physical programme (depending for example on the relative importance to be accorded to the interferometric and polarimetric signals). Figures 4 and 5 show examples of the calibration curves for the vertical chord #3. Figure 4 represents the Faraday angle as function of the time. Figure 5 shows the phase shift vs. the half-wave plate rotation.

From figure 5 it is clear that the value of the phase shift is not constant when the half-wave angle is varied, as it would be expected for a system with only ideal optical components. Because of this non ideal behavior, at JET the polarimetric signals are processed using a model which assumes that an unspecified optical element generates a “anomalous ellipticity” characterized by a constant phase shift referred to a rotated co-ordinate system of unknown orientation [6].

3.2 NEW CALIBRATION ALGORITHM

As mentioned, a new algorithm has been developed to extract more robust calibration parameters, valid over the whole range of JET discharges, from the signals acquired during the calibration [9]. In the new code all optical components, crossed by the laser beam for the vertical chords, have been modelled using the Mueller Matrix formalism. Referring to the polarimeter schematic for the

vertical chords reported in figure 2, the optical components involved in the model are: the half-wave plate, the wire grid located in front of the detectors and a cascade of the retarders to reproduce the "anomalous ellipticity", which afflicts the polarimetry measurements. Since a quite comprehensive analysis has shown that for chords 2 and 3 two retarders are enough, the discussion of this section will be particularised for this configuration of the equivalent model.

In ideal conditions, the wire grid should be at 45 degrees with respect to the propagation direction of the radiation, dividing the electric field into the directions x and y. Looking at the two detector signals, it is possible to estimate the angle between the wires and the incidence electric field of the radiation. As it is shown in figure 5, there is an angle of the polarization for which the phase shift equals 90 degrees and therefore tanf diverges to $\pm\infty$. Since this corresponds to a polarisation for which the R signal equals zero and therefore the p(t) signal equals zero, it means that all the radiation is collected by the i(t) detector. This condition is verified when the wires are parallel to the direction of p(t) signal. Then the position of the wire with respect to the incidence electric field can be estimated as:

$$\alpha_{WG2} = 90 - \alpha_0 \tag{22}$$

where α_0 is the angle corresponding to the singularity in figure 5. Since in the end the developed code implements only an equivalent model of the optical path, relation (22) is not always a completely satisfactory determination of the wire grid angle. Typically a small adjustment, of the order of a few degrees can be necessary to obtain the best results with plasma. This aspect has been taken into consideration in developing the real time version of the algorithm as will be discussed in the next sections.

After the wire grid , the laser beam is divided in two parts, reflected and transmitted, and the corresponding Stokes vectors are given by:

$$\vec{S}_{1,R} = M_R \cdot M'_{\delta 2} \cdot M'_{\delta 1} \cdot M'_{\alpha} \cdot \vec{S}_R \tag{23}$$

$$\vec{S}_{1,T} = M_T \cdot M'_{\delta 2} \cdot M'_{\delta 1} \cdot M'_{\alpha} \cdot \vec{S}_R \tag{24}$$

In equations (23) and (24), S_0 is the initial polarization of the laser beam and the Ms are the Mueller matrixes of the optical components used to model the optical path. The final Stokes vector ($\vec{S}_1$) is the combination of the two Stokes vectors (23) and (24).

Therefore, it is possible to know the polarisation angle and the phase shift, given by

$$\psi = \frac{1}{2} arctag\left(\frac{S_2}{S_2}\right) \tag{25}$$

$$\Phi = \frac{1}{2} arctag\left(\frac{S_3}{S_2}\right) \tag{26}$$

where S_1,S_2 and S_3 are the component of the final Stokes vector ($\vec{S}_1$).
These parameters are linked to the Faraday rotation angle (Ψ) and to the Cotton-Mouton effect (Φ) by:

$$\Psi = \psi - \Theta_0 \tag{27}$$

$$\Phi = \varphi - \phi_0 \tag{28}$$

All the details about this method to obtain the calibration constants of JET polarimeter can be found in [9].

To estimate the wire grid angle, the phase shift values (δ_1 and δ_2) and the angles at which the retarders are located (α_1 and α_2) in the Torus coordinate system (these are the quantities which define the matrixes in equations (23) and (24)), an optimization routine has been written in Matlab. For each chord, the routine finds the values of these quantities, which allow to best fit the phase shift curve and the HWP (half wave plate) position, shown in figure 5. This optimization routine is based on the lsqcurvefit Matlab function, which solves non-linear curve-fitting problems in the least-square sense.

In the following figures (6-7), an example of the fits of the experimental calibration curves obtained with the new calibration code are shown. The polarimetric measurements obtained with this new calibration algorithm in a wide range of plasma parameters has been reported in [9]. A systematic validation of the results has been performed with the method of the autocorrelation of the residua as documented in [10].

4. REAL TIME COMPATIBLE CALIBRATION ALGORITHM FOR SHOT-TO-SHOT ADJUSTMENT OF THE CALIBRATION FACTORS

The algorithms to interpret the data of the calibration procedure are meant to provide the parameters of the optical components used to model the various chords. In the case of the vertical chords #2 and #3 the unknown parameters are the 4 angles of the retarders ad the angular position of the wire grid, In general they can assume any value between 1 and 360 and therefore the number of combination is 3605. In the case of the chord #4, with 4 retarders the number of combination raises to 360^9. Of course the investigation of all these combinations cannot be performed in the interval before the plasma breakdown. Therefore a combined approach has been tested for JET. The parameters of the optical model are determined with an exhaustive scan of all the angles after the last manual calibration. Then on a shot to shot basis the values of the parameters are adjusted before the plasma breakdown. This is achieved with a limited scan on the various angles. A sensitivity analysis is to be performed to determine the appropriate range of angles to be scanned before every shot for each chord. The details will be discussed when the results for each chord are presented in the next sections. Found the reference points, an optimization function has been written to refine, shot-to-shot, the value of the unknown parameters with a resolution of 10-3 degrees.

5. IMPLEMENTATION OF THE CALIBRATION CODE FOR REAL TIME: VERTICAL CHORDS

As mentioned before, an on-line calibration, to link the output voltage of the detectors to the effective Faraday rotation angle, is carried out, for each chord, before each shot. For the chords #2 and #3, the optical components involved in the model are: the half-wave plate, the wire grid located in front of the detectors and a cascade of two retarders to reproduce the anomalous ellipticity, which afflicts the polarimetry measurements. Fixed the angle of the wire grid, the unknown parameters to be found with the calibration code are 4: the phase shift values and the angles at which the two retarders are located.

In this case, the optimization algorithm is able to refine the calibration in the phase of the shot before the plasma has been developed. A systematic investigation has shown that the range of angles to be investigated is ±8 degrees for the four parameters of the retarders and ±1 degree for the wire grid position.

This optimized function needs about 2 seconds to find the best values for the 4 unknown parameters, fixed the angle of the wire grid. This time has been estimated using a laptop with the following proprieties:

processor: Intel(R) Core(TM)2 DuoCPU T8100 2.10Ghz;
memory (RAM): 4Gb
operating system: 32-bit

Hence the time required is substantially shorter that the available time for the calibration. Even if also the angle of the wire grid is varied over the ±1 degree range, the computational time remains well below 10s, which is still compatible with the time available before plasma breakdown.

Once the calibration curves for the Faraday rotation and the Phase shift have been obtained, the experimental signals with plasma can be analyzed. In particular, for the vertical chords, it is possible to evaluate, in real time too, the density from the Cotton-Mouton measurements, because the toroidal field (B_t) is largely constant along the line of sight, and thus equation (2) can be rewritten as:

$$\Phi = k \cdot \lambda^3 \cdot B_t^2 \cdot \int n_e \cdot dz \tag{29}$$

and therefore the line-integrated electron density (n_e) can be directly obtained:

$$\int n_e \cdot dz = \frac{\Phi}{k \cdot \lambda^3 \cdot B_t^2} \tag{30}$$

with $l = 195\mu m$ and k, expressed in $^{rad}/_{mT}$, is equal to:

$$k = \frac{e^4}{16\pi \cdot c^4 m_e^3 \cdot \varepsilon_0} = 2.4 \cdot 10^{-11}$$

The results obtained for the vertical chords are reported in the next three subsections.

5.1 CHORD 3

To test the quality of the new code a statistical analysis have been carried out. As mentioned, the interferometer density has been used as reference to validate the results obtained with the new calibration.

The density estimated by the newly calibrated Cotton-Mouton phase shift is typically in very good agreement with the interferometric measurements as shown in figure 8 for a recent shot (79790).

Figure 9 shows the difference in fringes between the interferometer and the polarimeter density (1 fringe = 1.14×10^{19} m^{-2}) for 42 shots (79782-79817). This database comprises shots after a single manual calibration. Therefore the reference point for the optical model is the same (see section 4). For each shot the automatic procedure to adjust the calibration values has been run. As we can see, from figure 9 the difference between the interferometer and the polarimeter estimates of the density is always approximately between ±1 fringe. It is noteworthy that the points, for which the discrepancy exceeds ±1 fringe, are typically at the end of the discharge during the ramp down of the current when the polarimetric signals are very low and the S/N ratio decreases significantly. The new upgrades of the diagnostics should improve this situation to a large extent.

In figure 10, the absolute value of the polarimeter density is plotted versus the absolute interferometer density. The linear relation between the two is satisfactory. It is also interesting to note that this agreement extends over a range of more than an order of magnitude (from less than $1\cdot10^{19}$ to more than 10^{20} m^{-2}). This is an important fact confirming the quality of the adopted approach. Indeed, as mentioned, the calibration reference point is the same over the entire range of densities, proving the potential of the optical model developed. No manual intervention is required to adjust the calibration even over a range of densities exceeding an order of magnitude. Previous calibration techniques required a complete revision of the fitting procedures over intervals of densities a fraction of the one considered in this example. The small variations in the optical parameters, implemented by the automatic refinement procedure, take into account the small variations in the diagnostic settings which occur between shots and are an unavoidable aspect of the present design of the diagnostic.

It is worth mentioning that the developed method allows converging on an optical model of the diagnostic, which interprets properly not only the phase shift but also the Faraday rotation. The same procedure provides a unique set of parameters, which provides also a coherent interpretation of the Faraday rotation and not only of the density. This is shown in figure 11, in which the Faraday rotation for shot 77650 is compared with the same quantity estimated by the best available propagation code base on the Stokes formalism [9]. This code use the magnetic fields estimated by EFIT and the density profile of the Thomson scattering to calculate the evolution of the polarization state of the laser beam crossing the plasma.

5.2 CHORD 2

The equivalent optical model for the chord #2 is the same as the one developed for the chord #3.

Again it consist of two retarders before the final wire grid. With this optical model it is possible to fit quite well the calibration curves obtained after a manual calibration. The reference point for the calibration used in the last shots of the 2009 (79844) has been found and the quality of the fits is reported in figure 12.

During the last campaign of 2009, different manual calibrations have been performed, thus it has not been possible to perform a complete statistical analysis as for chord 3. In any case no particular problem is expected to rise for chord 2, because its topology is very similar to chord 3 and it has been proved that the same optical model, with only two retarders, one wire grid and an halfwave plate, is adequate. Examples of results obtained for chord 2 are reported in the following figures 13 and 14. They include a series of 13 shots after a manual calibration. The same algorithm as the one used for chord 3, to refine the calibration in the phase of the shot before the plasma, has been applied. It has been double-checked that the appropriate range of angles to be covered is ±8 degrees for the four parameters of the retarders and ±1 degree for the wire grid position, exactly as for chord 3.

The slightly poorer agreement between the polarimetric and the interferometric measurements of the line integrated density, compared to chord 3, are to be attributed to the lower quality of chord 2 signals available and not to the calibration algorithm. In any case, the quality of the polarimetric estimates are considered more than adequate for real time applications.

5.3 CHORD 4

After studying a wide set of shots, for this chord the optical model has been modified compared with the one developed for the vertical chords #3 and #4. Indeed it has resulted impossible to obtain a good fitting of the calibration curves with an optical model consisting of only two retarders, an half-wave plate and a wire grid. To properly model the manual calibrations, two additional retarders have to be added. This improves a proper fitting of the calibration curves as shown in figure 15, which compares the results obtained with a model with 2 and one with 4 retarders.

Given the need of inserting these two additional retarders, a new sensitivity analysis had to be performed to determine the intervals over which the various optical parameters have to be scanned in the automatic procedure to be run before each shot. A preliminary investigation has shown that the various parameters have to be scanned over the range ±8 degrees for the six parameters of the retarders and ±1 degree for the wire grid position. The following figure 16 shows the good quality of the results obtained with this optical model and the devised automatic procedures. The difference between the polarimetric line integrated density and the interferometric is reported for 14 discharges, showing that the difference is almost always below one fringe. The higher discrepancies occur toward the end of the discharges, when the Signal to noise ratio of the phase shift measurements is typically quite low.

The recourse to two additional retarders provides quite good results. On the other hand, it has to be mentioned that this makes much more lengthy to converge on the new calibration parameters in the interval before the breakdown of the plasma. Up to 10 seconds can be necessary for the

algorithm to converge. Moreover, the range of variable to analyse renders more difficult to identify the reference point of the chord. The number of combination (3608 angles for the 4 retarders) increases exponentially rendering even more prohibitive to determine the reference point manually.

6. NEW CALIBRATION CODE FOR THE LATERAL CHORDS

The following figure shows the layout of a lateral chord of JET Polarimeter.

From figure 17, it is clear that is not possible to apply directly the calibration code, developed for the vertical channels, to the horizontal lines of sights because the laser path for the lateral chords is different.

In this case, the radiation passes through the plasma and then it is reflected back using a mirror located on the inner wall. So, in the calibration code this additional optical component has been introduced, which is described by the following Mueller matrix:

$$M_{\varepsilon} = \begin{vmatrix} 1 & 0 & 0 & 0 \\ 0 & \cos 2\varepsilon & \sin 2\varepsilon & 0 \\ 0 & -\sin 2\varepsilon & \cos 2\varepsilon & 0 \\ 0 & 0 & 0 & 1 \end{vmatrix} \tag{31}$$

that represents the matrix of an ideal rotator. In the case of the polarimeter lateral chords it has been found that the matrix of an ideal mirror, with ε equal to 180 degrees, is more than adequate to obtain satisfactory results.

The other components involved in the model are the same considered for the vertical chords: the half-wave plate, the wire grid located in front of the detectors and the retarders introduced to reproduce the "anomalous ellipticity". Again in the following the treatment is particularised for two retarders since this is a sufficiently general situation without unnecessary complications.

So, for the horizontal chords, the Stokes vectors after the wire grid (WG2) are given by:

$$\vec{S}_{1,R} = M_R \cdot M'_{\delta 2} \cdot M'_{\delta 1} \cdot M'_{\alpha} \cdot \vec{S}_R \tag{32}$$

$$\vec{S}_{1,T} = M_T \cdot M'_{\delta 2} \cdot M'_{\delta 1} \cdot M'_{\alpha} \cdot \vec{S}_R \tag{33}$$

where the matrices $M_T, M'_{\delta 2}, M'_{\delta 1}$ and M_{α} are the same as the ones seen in the previous section. Since the only difference with respect to the vertical chords is the presence of the mirror, which can be easily modelled with a fixed Mueller matrix, the new calibration procedure and the subsequent elaboration of the raw data, to evaluate the Faraday rotation and the phase shift angle, are the same as for the vertical channels. Again only four quantities (the phase shift values δ_1 and δ_2 and the angles at which the retarders are located α_1 and α_2) have typically to be determined with a series of scans before the breakdown.

7. LINE INTEGRATED DENSITY IN REAL TIME THEORY AND APPROXIMATIONS

The plasma density is definitely one of the most important physical parameters to be controlled during a plasma pulse in a tokamak. The approximations to calculate the line integrated density profile starting from the polarimetric measurements for the vertical chords are well-known. On the other hand, no consolidated formula is available to calculate in real time the line integrated density the horizontal channels.

Using the Stokes vector formalism, the Faraday angle and the Phase Shift can be expressed in the following way [9]:

$$\tan(2\psi) = C_1 \int_0 n_e B_r dr \tag{34}$$

$$\tan(2\phi) = \frac{-C_2 \int_0 n_e B_t B_p dr}{\tan 2\psi} \tag{35}$$

with $C_1 = 2 \times 10^{-20}\ m^{-2}\ T^{-2}$ and $C_2 = 1.794 \times 10^{-22}\ m^{-2}\ T^{-2}$ (according to the JET laser wavelength $\lambda = 195\mu m$).

Since the objective is to calculate the line integrated density, relations (35) and (36) have to be simplified and expressed in terms of quantities which can be provided in real time. To this end, all the various quantities can be taken out of the integrals (except n_e) and the profiles effects can be absorbed in an empirical constant. The following approximations for the radial magnetic field (B_r) and the poloidal magnetic field (B_p) can be considered:

$$B_r \propto I_p B_t \Rightarrow \int_0 n_e dr = k_1 \frac{\tan(2\psi)}{I_p B_t} \tag{36}$$

$$B_p \propto I_p \Rightarrow \int_0 n_e dr = k_2 \frac{\tan(2\psi) \cdot \tan(\phi)}{I_p B_t} \tag{37}$$

where K1 and K2 are constants that have to be determined empirically.

The K1 constant, in equation 36, is given by the ratio of the integrated density and the term on the right side of relation 36. The constant K1 is therefore just the angular coefficient m of the linear equation:

$$y = mx \qquad \text{where} \qquad \begin{cases} y = \int_0 n_e dr \\ m = k_1 \\ x = \dfrac{\tan(2\psi)}{I_p B_t} \end{cases}$$

For each pulse, the range of times between 40s and 44s, when the gradient of the physical parameters are higher , is scanned and then K1 calculated by a linear fit of these points. The chosen range of times is due to the fact that, during the rise of the plasma current, a wider range of angles is scanned whereas during the flat top the Faraday rotation remains more constant. Therefore the beginning

of the discharge provides better data for a fit of the constant K_1. Moreover, obtaining K_1 during the first seconds of the shot would give the opportunity to implement a shot to shot estimate of the constant K_1. It is indeed possible to conceive to use the value of K_1 determined for the previous shot during the rise of the plasma current and then update the value of the constant with the new fit obtained during the rise of the current.

The same approach has been used to evaluate the constant K_2 in equation 37.
Since we want to obtain general empirical-constants to be used in real time to get the integral density using the above expressions, K_1 and K_2 should be calculated using a large database of shots. This has been possible only for the constant K_1 since the signal of the phase shift is typically very low for the horizontal chords. So K_2 has been preliminarily estimated only for a couple of shots with a sufficiently robust signal of the Cotton Mouton phase shift.

7.1 LINE INTEGRATED DENSITY FOR CHORD 5

In Figure 18 an example of the range of times considered (blue line) for the analysis of the physical quantities of interest is shown.

In Figure 19 the fit obtained for the K_1 constant from the experimental points of the range of times considered, for the same pulse as in Figure 1, is shown.

In Figure 20 the line integrated density, calculated with the K_1 value, is compared to the interferometer density.

The calculation has been performed for 27 shots, the obtained values have been averaged obtaining a mean value of the constant $\langle K_1 \rangle$:

$$\langle K_1 \rangle = (9.9 \pm 1.4) \cdot 10^{26}\ \mu^{-2}\ T^{-2}\ A^{-1} \tag{39}$$

Using this value in the expression (36), the integral density has been calculated for the same 27 shots (in the range from 68698 to 79853), together with the modulus of the difference between the obtained values and the interferometer line integrated densities. The results are shown in the following figure 21.

As it can be seen in the previous figure 21, the line integrated density obtained with the present approximation differs from the interferometric measurements typically significantly less than a fringe. Therefore we can say there is a quite good agreement between the two density estimates particularly for real time applications. Again the bigger discrepancies occur at the end of the discharge, when the polarimetric signals are very low.

In Figure 22 it can be seen how this level of accuracy is maintained for the entire range of JET densities, since the shots analysed cover about an order of magnitude range of densities.
It is interesting to underline the usefulness of the expression (36), since it provides a reliable signal without the drawback of fringe jumps. This can be seen, for instance, in Figure 23.

In figures 24 and 25, the quality of the second approximation (equation 35), for the only five

shots in which a good signals were available together with a proper calibration, is shown.

This first study shows that the Faraday angle rotation and the phase shift, provided by the Polarimeter of the JET tokamak, can be used to calculate the plasma line integrated density in real time with an accuracy of better than one fringe.

This can be done by the two relations (34) and (35) previously discussed, using the toroidal field (B_t) data and the plasma current (I_p) data only.

While it has been possible to make a quite satisfactory statistical validation of expression (36) involving only Faraday-effect data, expression (37) has been just verified only for the two shots with reliable Cotton-Mouton effect signals. On the other hand, given the more solid theoretical background of relation (37), it would be nice to test and implement it because it is expected to provide even better results. If the upgrade of the diagnostic will provide the expected improvements in the signal to noise ratio of the phase shift measurement for the horizontal chords, the approximation (37) could be tested systematically.

7.2 LINE INTEGRATED DENSITY FOR CHORD 7

The same analysis shown for the chord 5 in the previous section, has been performed for the chord #7. First of all, it has been necessary to evaluate the constant in the relation 36, following the same procedure explained above.

The calculation has been performed for 24 shots, the obtained values have been averaged obtaining an average value of the constant $\langle K_1 \rangle$:

$$\langle K_1 \rangle = (11.92 \pm 1.4) \cdot 10^{26}\ \mu^{-2}\ T^{-2}\ A^{-1} \tag{40}$$

Using this value in the expression (36), the integral density has been calculated for the same 24 shots, together with the modulus of the difference between the obtained values and the interferometer line integrated densities. The results are shown in the following figure 26.

Again, the line integrated density obtained with the present approximation differs from the interferometric measurements typically significantly less than a fringe. Therefore we have a quite good agreement between the two density estimates particularly for real time applications. Even in this case, the bigger discrepancies occur at the end of the discharge, when the polarimetric signals are very low.

In Figure 27 it can be seen how this level of accuracy is maintained for the entire range of JET densities, since the shots analysed cover about an order of magnitude range of densities.

8. APPLICATIONS OF THE POLARIMETRIC MEASUREMENTS IN REAL TIME

The availability in real time of reliable polarimetric measurements opens new prospects to the feedback control of Tokamak plasmas. For the purpose of machine protection, the measurement of the line integrated density without fringe jumps from the cotton Mouton effect is a quite important

improvement. The control of density would become more reliable and the exploitation of the machine more efficient, since discharges will not have to be terminated simply for the unavailability of the interferometric measurement. In the case of the protection of the wall against the neutral beam shine through, this upgrade is considered particularly relevant now that JET will have to operate with a full metallic wall. Moreover in general the magnetic reconstruction will benefit from the Faraday rotation measurements. Indeed, it has already demonstrated with a systematic analysis that internal measurements of the fields, either with MSE or polarimetry, are essential in a Tokamak to identify the proper equilibrium, since the external magnetic coils alone are not enough to identify the right solution [1].

In the last years, it has become quite evident that the constraints of polarimetry on the equilibrium can have a significant effect also on the determination of the plasma boundary. In this respect an important example is the following comparison of the various topological parameters, at the edge and in the core of the plasma, obtained with EFIT using the magnetic pickup coils only and with EFTF, the version of EFIT using also the polarimetric measurements of chords 2,3,5 and 7. To summarise the results of the comparison the attention has been focused on the parameter ROG, which measures the plasma wall distance in the outer equatorial plane, the coordinates Z_{mag} and R_{mag} of the magnetic axis and the value of the safety factor q_{95} at 95% of the plasma radius. In figure 28, the time evolution of these quantities is shown for a well diagnosed discharge. The estimates of EFTF can differ even of a couple of centimetres with respect to the values provided by EFIT with the magnetic only. This discrepancy is quite significant and the fact that the EFTF measurements are more accurate as been verified using other diagnostics such as the cameras looking at the plasma edge. The edge safety factor can also be significantly different between the two estimates (see also later).

With regard to the more general problem of profile control, polarimetry has also been the reference internal measurement for advance experiments such as the control of the q profile [11]. To improve the quality of the internal magnetic topology a new equilibrium code has been developed for JET explicitly for this purpose. This new code is called EQUINOX and has been designed and implemented in C++ using a finite element method and a non linear fixed point algorithm associated to a least square optimization procedure [12]. The code relies on tokamak specific software to provide flux values on the first wall of the vacuum vessel. By means of least-square minimization of the difference between measurements and the simulated ones the code identifies the source term of the non linear Grad-Shafranov equation. The experimental measurements that enable the identification are the magnetics on the vacuum vessel, the interferometric and polarimetric measurements on several chords and the motional Stark effect measurements. Since the algorithm is initialized from the equilibrium at the previous time step, two or three point iterations are usually enough to ensure convergence. This leads to a very efficient and robust algorithm.

Recently the code has been systematically validated and it is ready to run in the framework of JET real time system. An example of the importance of the magnetic internal measurements to converge on the equilibrium is shown in figure 27, in which the EQUINOX estimates are also

compared with the established EFIT reconstructions.

Figure 29 prove very clearly that the constraints provided by the polarimetric measurements are essential to obtain realistic current distributions at least for non monotonic q profiles.

CONCLUSIONS

The increasing sophistication of the control strategies for both plasma protection and physics experiments in JET has motivated a revision of the calibration procedures of the polarimeter. The aim is to provide accurate calibration constants in the interval between the beginning of the on line calibration and the plasma breakdown. If successful, this approach would allow providing accurate polarimetric measurements in real time on a shot to shot basis for the operational space of JET.

To this end, a new calibration algorithm has been refined and optimised, to interpret the calibration measurements in the time interval allowed for the data processing before a discharge. For the vertical chords, the results obtained for the line integrated density, based on the well known formula for the Cotton-Mouton effect, are within one fringe of the reference interferometer measurements. The estimates of the Faraday rotation have been successfully verified with the most used propagation code available. In order to validate the horizontal chords, new approximate formulas have been derived, which provide the line integrated density from the Faraday rotation and the phase shift measurements. The estimates of these approximated formulas are more than satisfactory, since they provide an estimate of the line integrated density within one fringe of the interferometric density for the whole operational range of JET. These results open new perspectives for the use of polarimetry in real time also for machine protection purposes, such as the control of the neutral beam shine through. With regard to more scientific plasma control experiments, the new shot to shot calibrated polarimetric measurements are planned to be used extensively as constraints for the code EQUINOX, This code implements a solution of the Grad-Shafranov equation providing the entire topology of the magnetic field in times compatible with the time requirements for the control of the current profile. The version of the code using the polarimetric measurements has already been validated and is ready to be deployed in real time during the next campaigns. Given the significant improvements of the interferometer polarimeter of JET being implemented, which should significantly improve the signal to noise ratio of the measurements, a routine use in real time of the properly calibrated Faraday rotation and phase shift is expected to materialise since the beginning of the next campaigns.

ACKNOWLEDGMENTS

This work, supported by the European Communities under the contract of Association between EURATOM and ENEA/CEA, was carried out under the framework of the European Fusion Development Agreement. The views and opinions expressed herein do not necessarily reflect those of the European Commission.

REFERENCES

[1]. F.S. Zaitsev, D-P-Kostomarov and E.P. Suchkov "Existence of substantially different solutions in an inverse problem of plasma equilibrium reconstruction" 35th Plasma Physics Conference, 2008, P-1-091

[2]. L. Laborde et al "A model-based technique for integrated real-time profile control in the JET tokamak" Plasma Physics and Controlled Fusion **47** (2005), 155-183

[3]. A. Murari et al "Real Time Recovery of the Electron Density from Interferometric Measurements affected by Fringe Jumps" Review of Scientific Instruments **77**, 073505 (2006)

[4]. De Marco F and Segre S.E. 1977, Opt. Commun, 23, 125.

[5]. K. Guenther, Proceedings of the 31st EPS, P5-172, 2004

[6]. K. Guenther and JET-EFDA Contributors, Plasma Physics and Controlled Fusion **46**, 1423 (2004).

[7]. D. Véron "Submillimeter Interferometry of High-Density Plasmas", "Infrared and Millimeter Waves", Vol.2 Instrumentation, Ed. K. J. Button, Academic Press, 1979.

[8]. M. Gelfusa, M. Brombin, P. Gaudio, A. Boboc, A. Murari, F. P. Orsitto, "Modelling of the signal processing electronics of JET interferometer-polarimeter" Nuclear Instruments and Methods in Physics Research, In press (Available online 6 March 2010).

[9]. M. Gelfusa, A. Murari, P. Gaudio, A. Boboc, M. Brombin, F.P. Orsitto, E. Giovannozzi, "A new calibration code for JET polarimeter" Review of Scientific Instrument, **81**, 053507 (2010).

[10]. M. Gelfusa, A. Murari, D. Patanè, P. Gaudio, A. Boboc, "Validation of JET polarimetric measurements with residual analysis" accepted for publication in Measurements Science and Technology, (2010).

[11]. M. Born and E. Wolf, Principles of Optics, Pergamon Press, Oxford, 1980.

[12]. D.S. Kliger, J.W. Lewis, C.E. Randall, Polarized Light in Optics and Spectroscopy, Academic Press, USA, 1990.

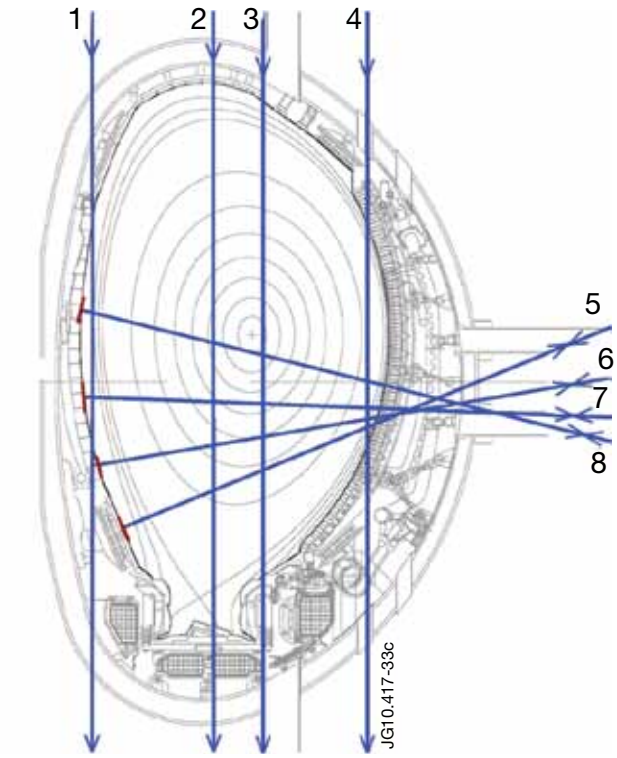

Figure 1: Layout JET interferometer-polatimeter

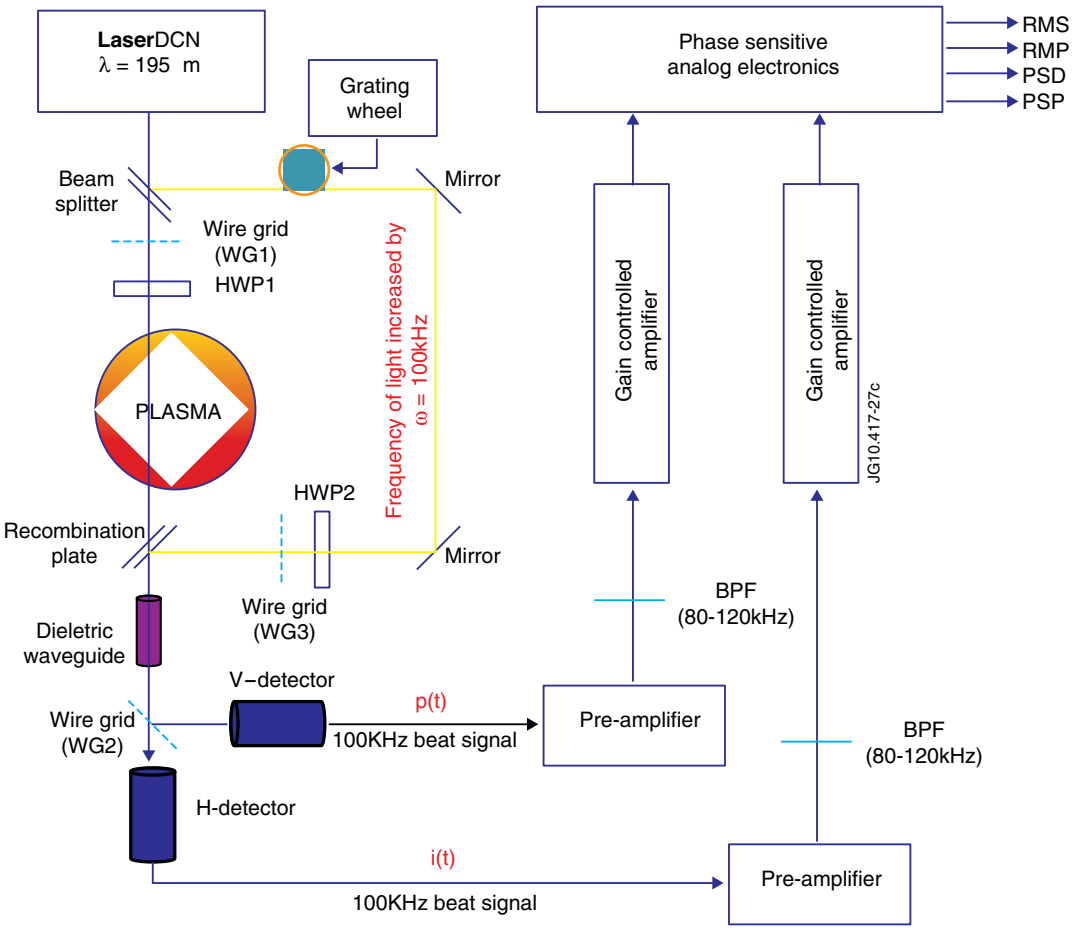

Figure 2: Schematic of the Polarimeter vertical chords.

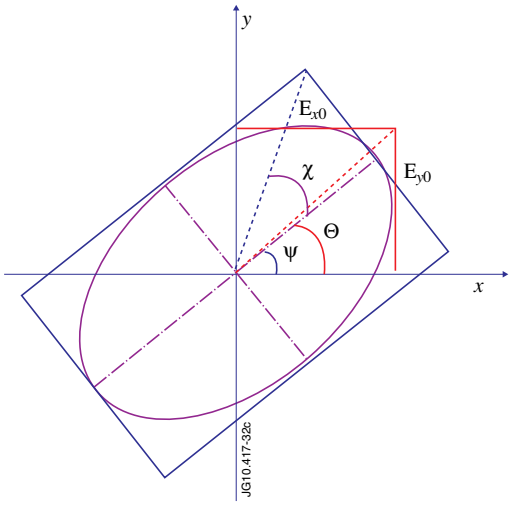

Figure 3: The polarisation ellipse is often adopted to understand the relation between the electrical and the geometrical parameters of the polarised radiation.

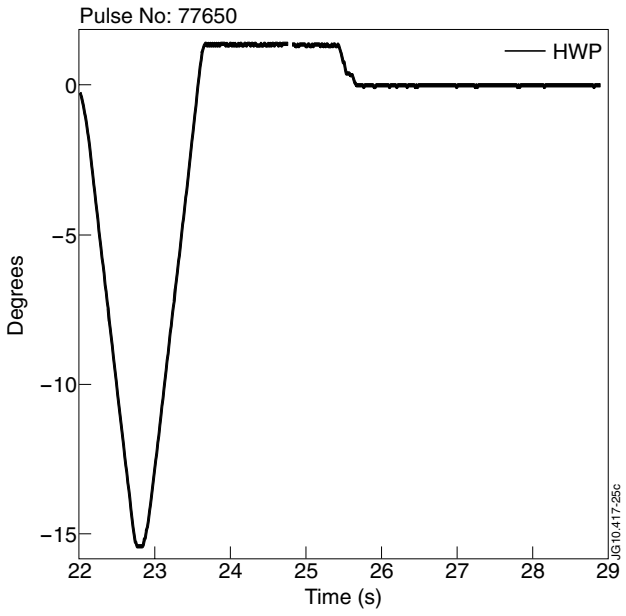

Figure 4: Calibration curve of the Faraday rotation (Pulse No: 77650 chord #3). The error bar on the Faraday rotation is of the order 0.2 degrees.

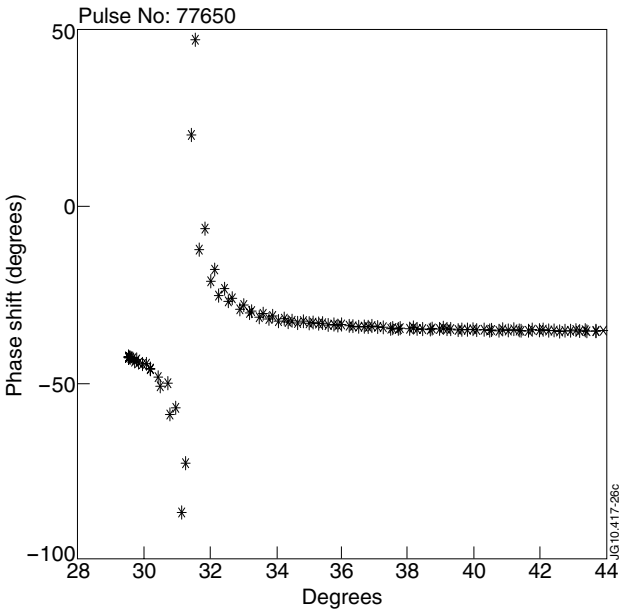

Figure 5: Phase shift calibration curve (Pulse No: 77650 chord #3). The error bar on the Phase shift is of the order 2 degrees.

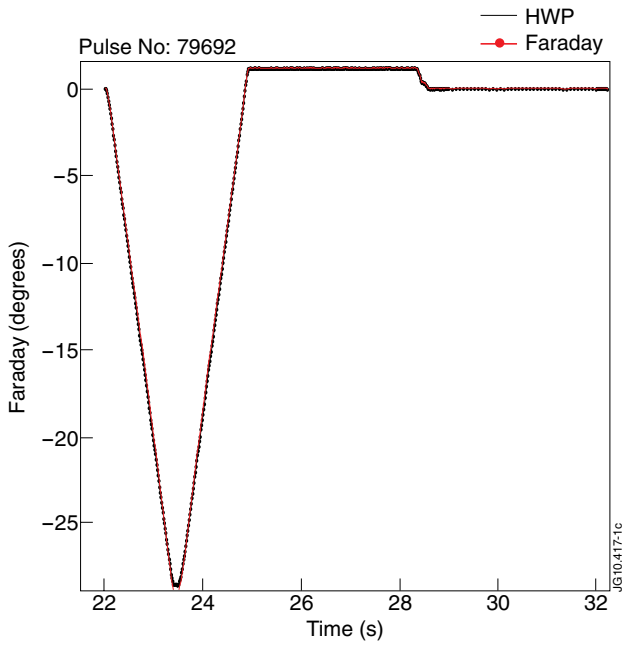

Figure 6: Comparison between the experimental calibration curve (black dotted line) and the estimate of the new calibration model (red dotted line). Pulse No: 79692 chord #3.

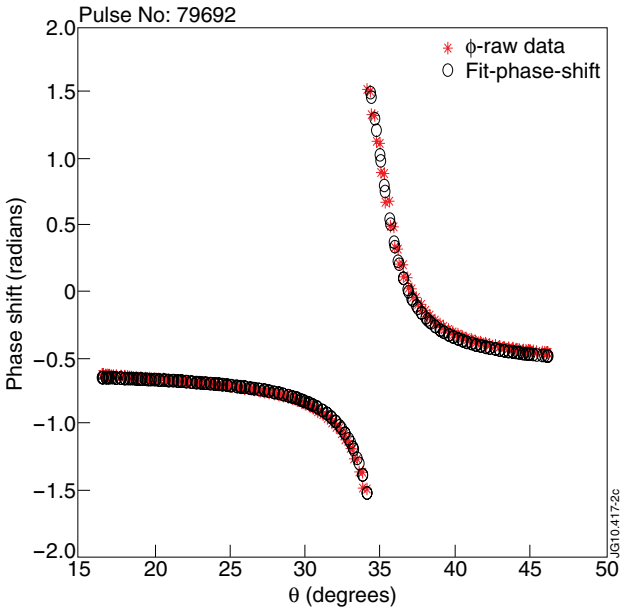

Figure 7: Phase shift calibration curve (Pulse No:79692 chord #3). Comparison between the experimental calibration curve (black dotted line) and the estimate of the new calibration model (red dotted line).

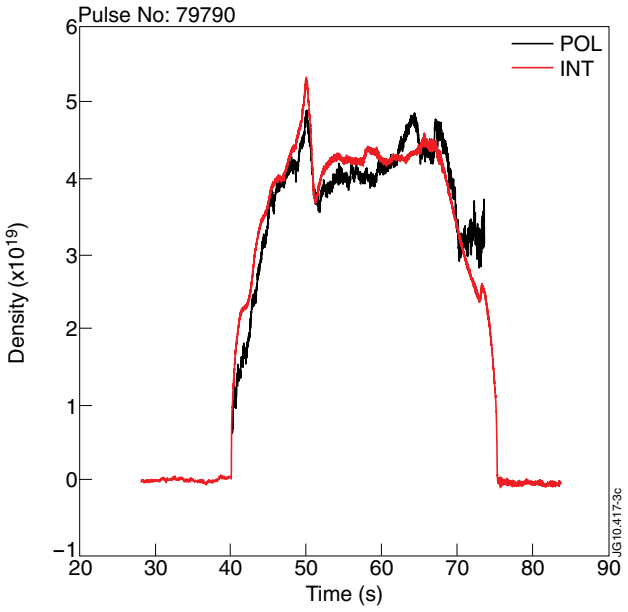

Figure 8: Comparison between the density with the new calibration (blue line) with the interferometer (red line). Pulse No: 79790.

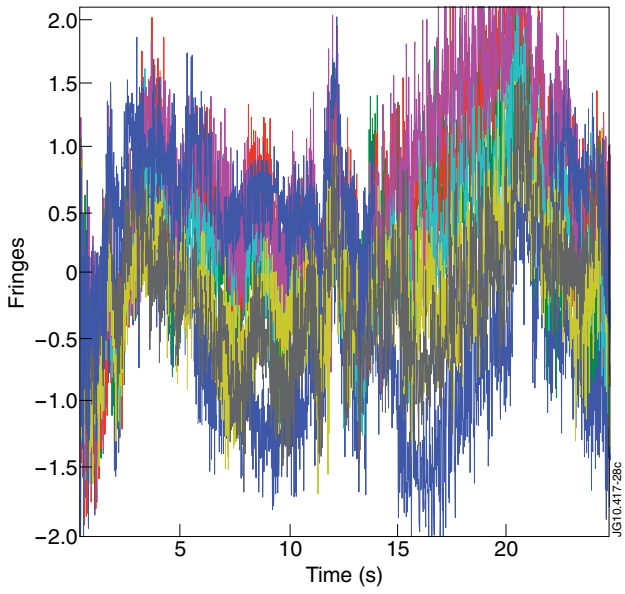

Figure 9: Difference in fringes between the interferometer and the polarimeter density.

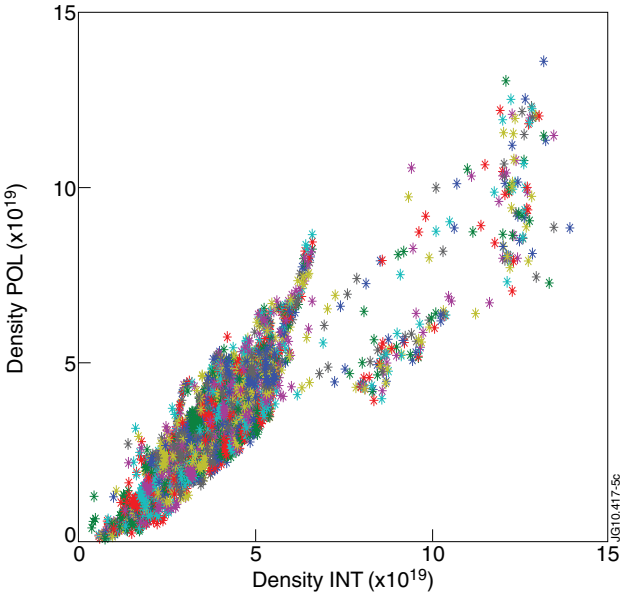

Figure 10: Polarimeter density Vs Interferometer density.

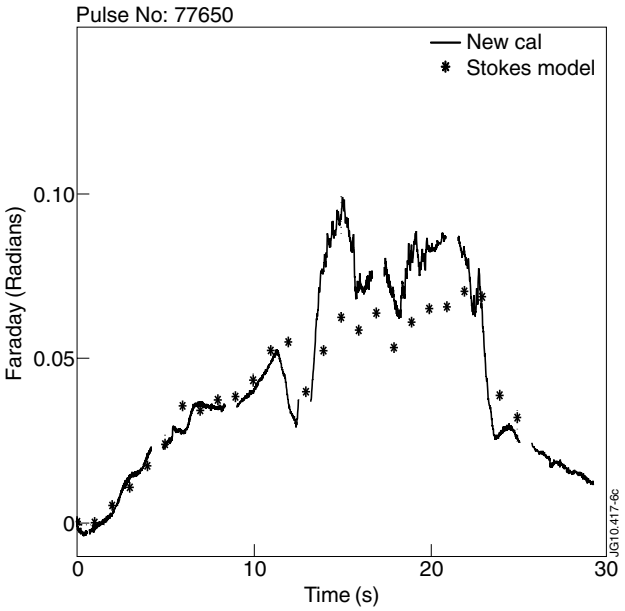

Figure 11: Comparison of the experimental Faraday rotation obtained with the described calibration procedure and the one calculated by a propagation code implementing the Stokes formalism and using EFIT estimate of the fields for chord 3.

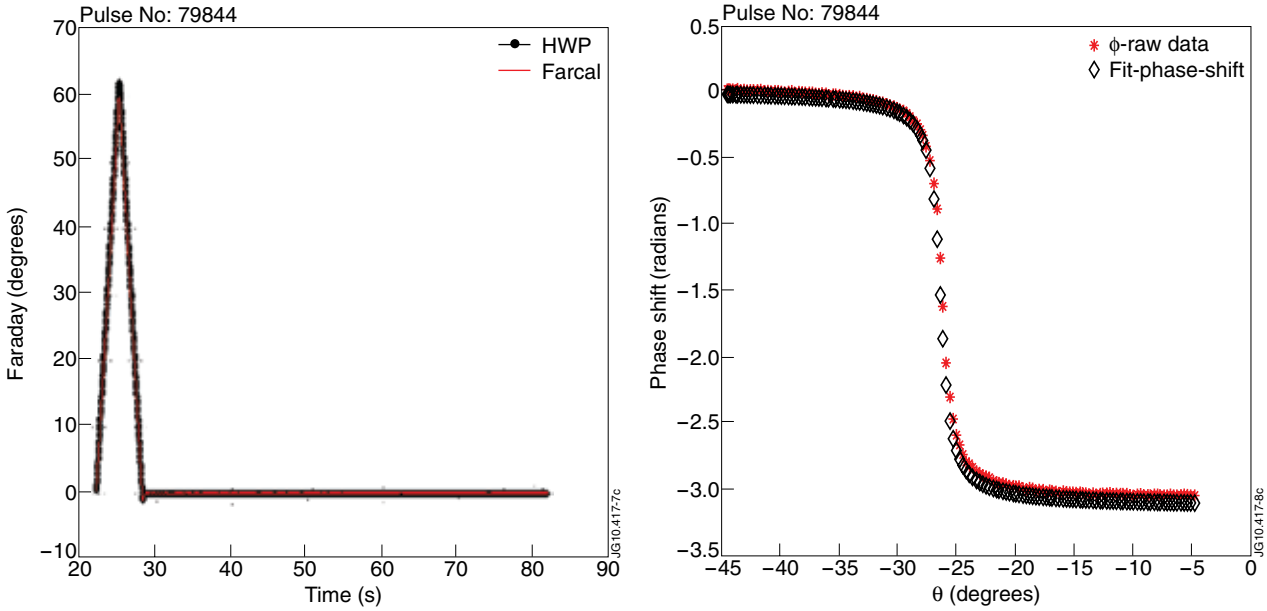

Figure 12: Calibration curves and their fit for chord 2. Left: Faraday angle. Right: Phase Shift.

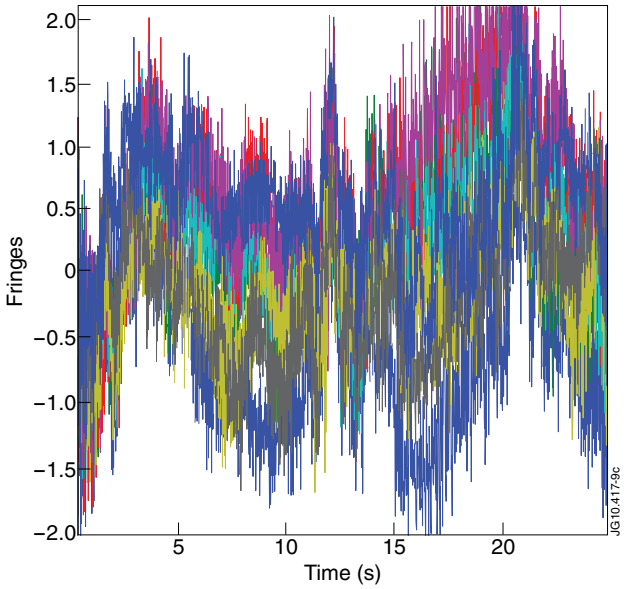

Figure 13: Difference in fringes between the density estimates of interferometry and polarimetry for chord 2.

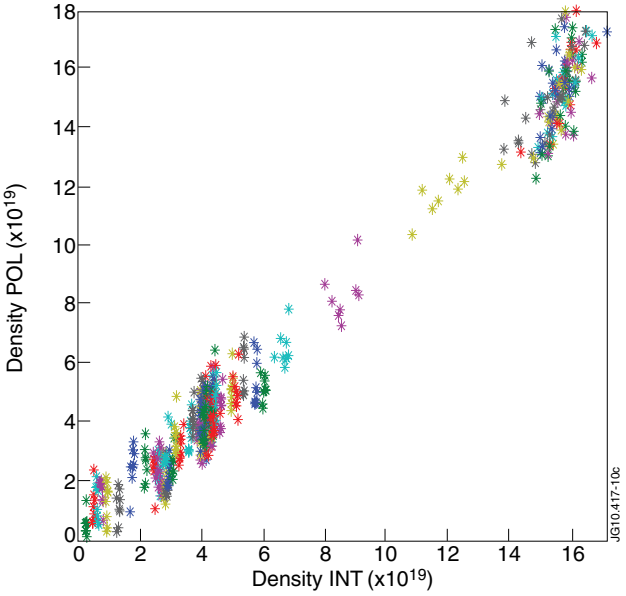

Figure 14: Polarimetric density versus interferometric density.

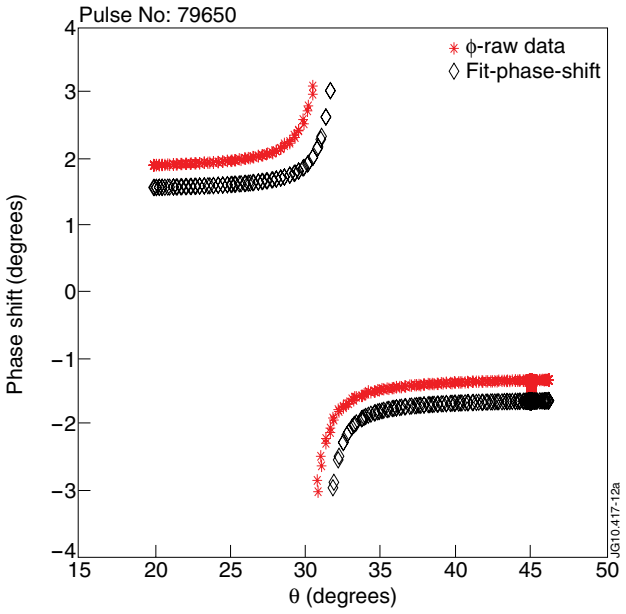

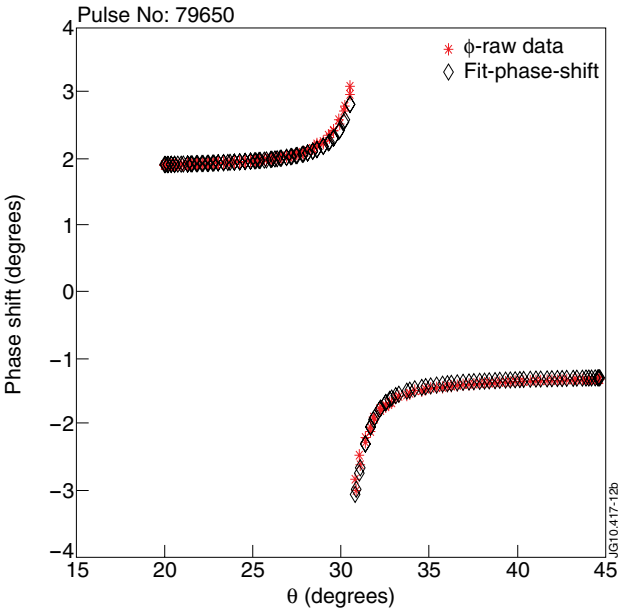

Figure 15: Calibration curves and their fit for chord 4. Left: optical model with 2 retarders. Right: optical model with 4 retarders.

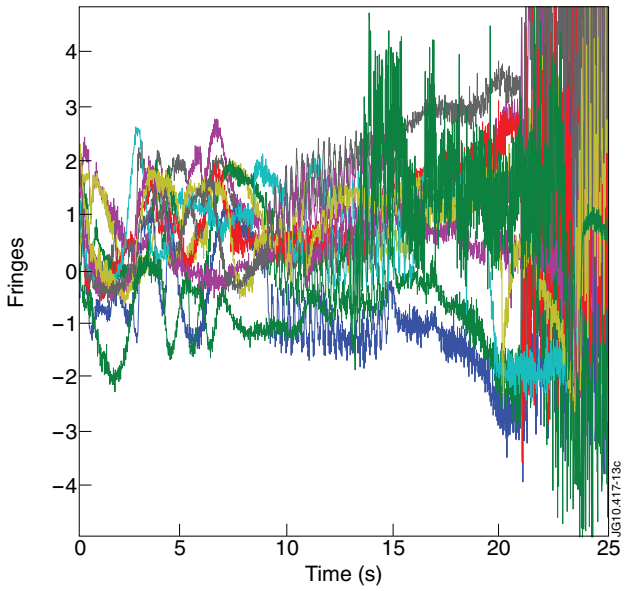

Figure 16: Difference in fringes between the density estimates of interferometry and polarimetry for chord 4.

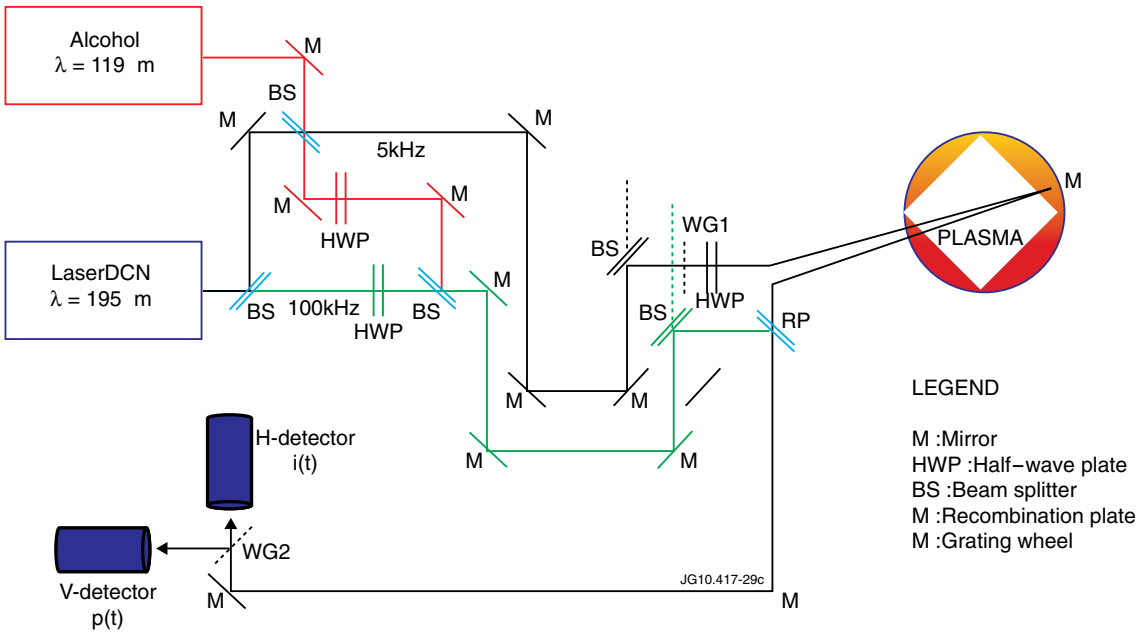

Figure 17: Schematic of the Polarimeter horizontal chords.

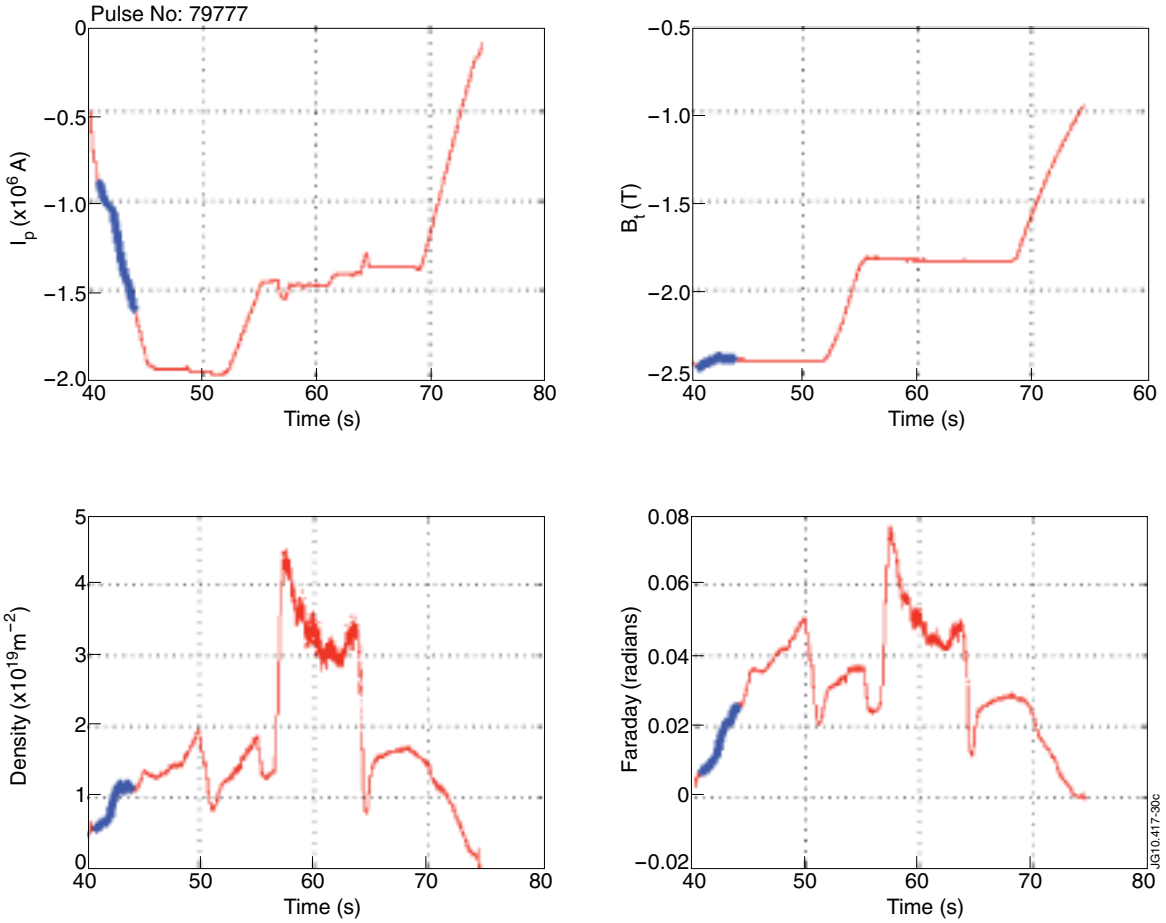

Figure 18: Variation of the main parameters used in the approximated equation (36) to provide the line integrated density. The blue part of the curves is the interval used to fit the experimental quantities.

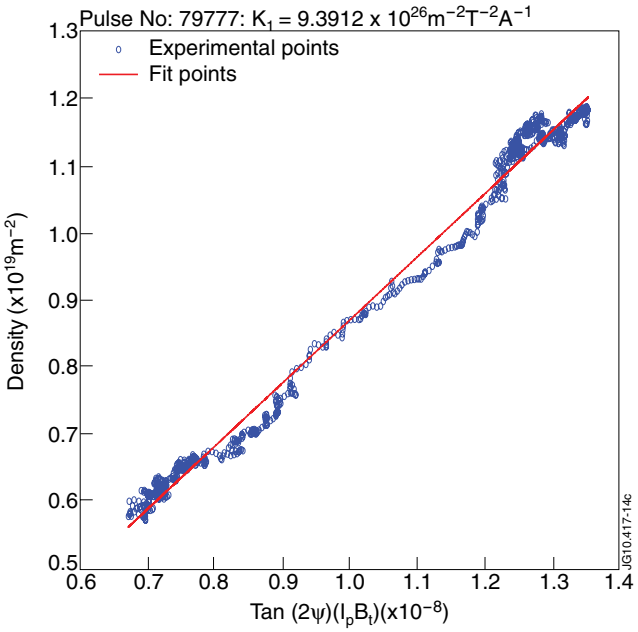

Figure 19: Determination of the constant K1 for a shot .

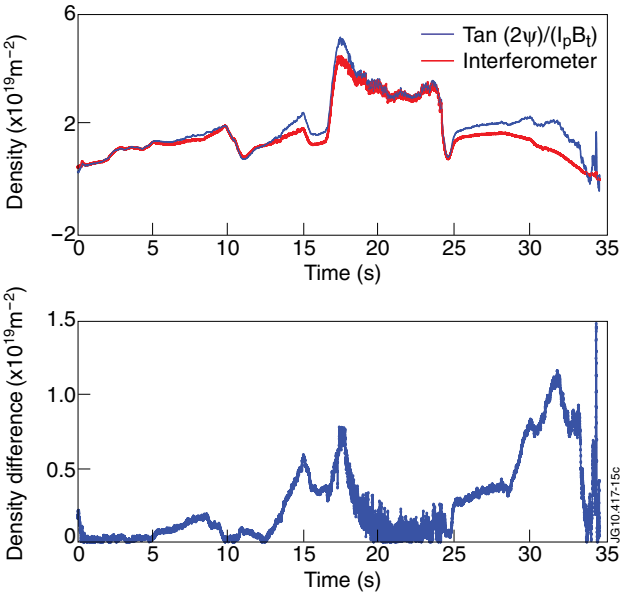

Figure 20: Comparison of the interferometric density and the density calculated on the basis of equation (36) for one shot. In the bottom plot the difference between the two estimates.

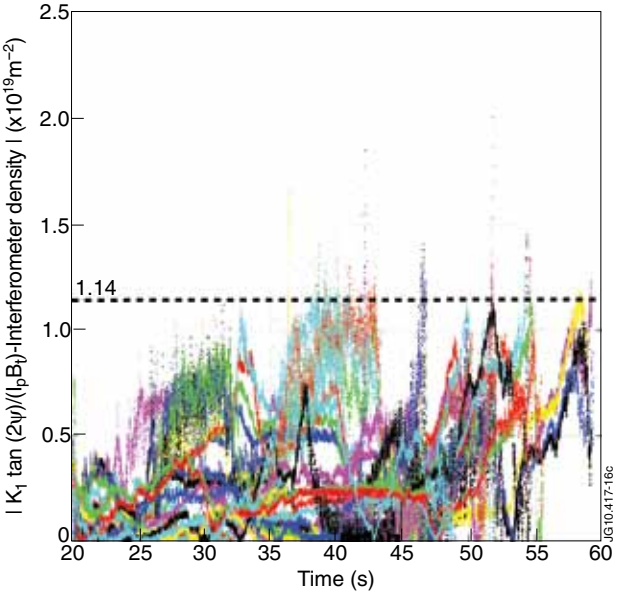

Figure 21: Statistical comparison of the interferometric density and the density calculated on the basis of equation (36) for chord 5.

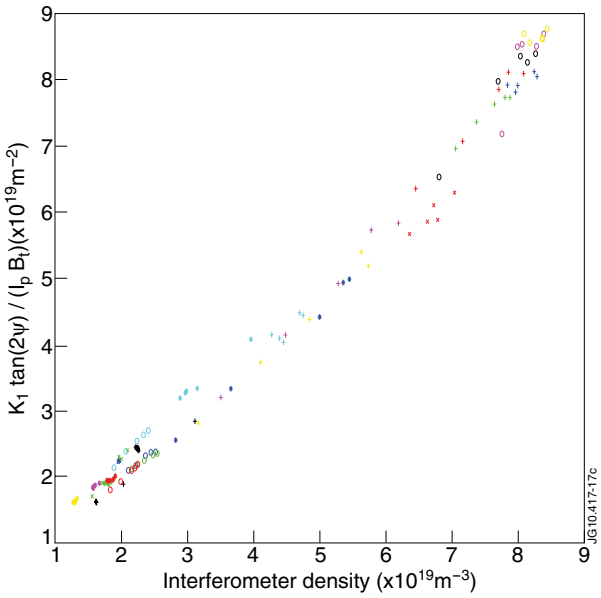

Figure 22: Polarimetric density estimated with equation (36) versus the interferometric measurements.

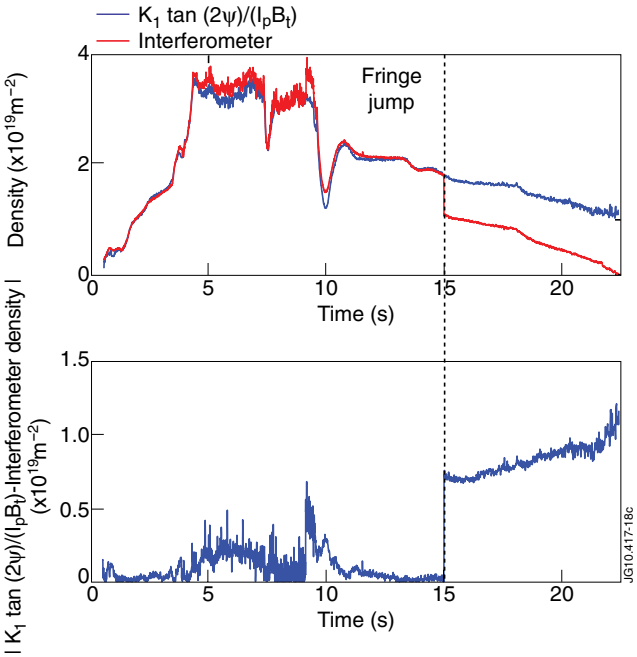

Figure 23: Comparison of the interferometric density and the density calculated on the basis of equation (36) for one shot. The robustness of the polarimeric signal is clear whereas the interferometer presents a fringe jump.

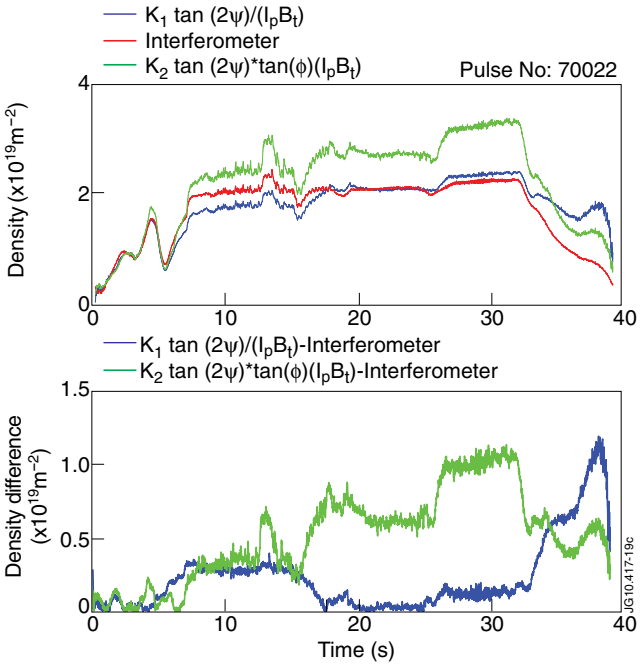

Figure 24: Comparison of the interferometric density and the density calculated on the basis of equation (37) for Pulse No: 70022. In the bottom plot the difference between the two estimates.

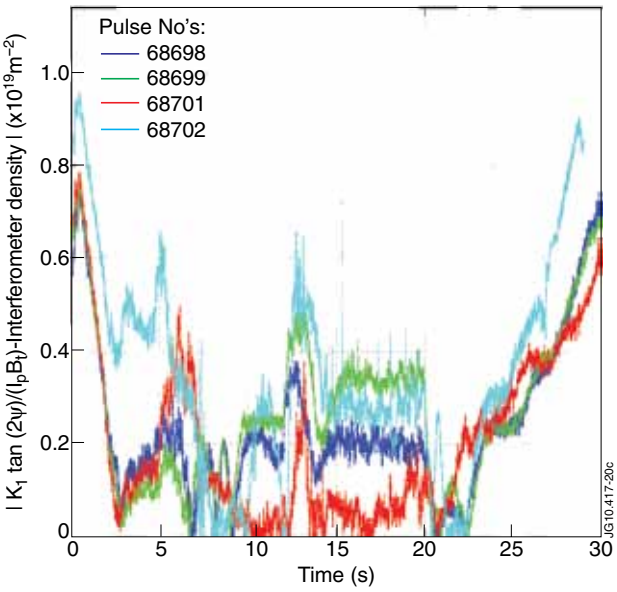

Figure 25: Statistical comparison of the interferometric density and the density calculated on the basis of equation (37). The accuracy of this approximation is well within one fringe (1.14 $10^{19}m^{-2}$)

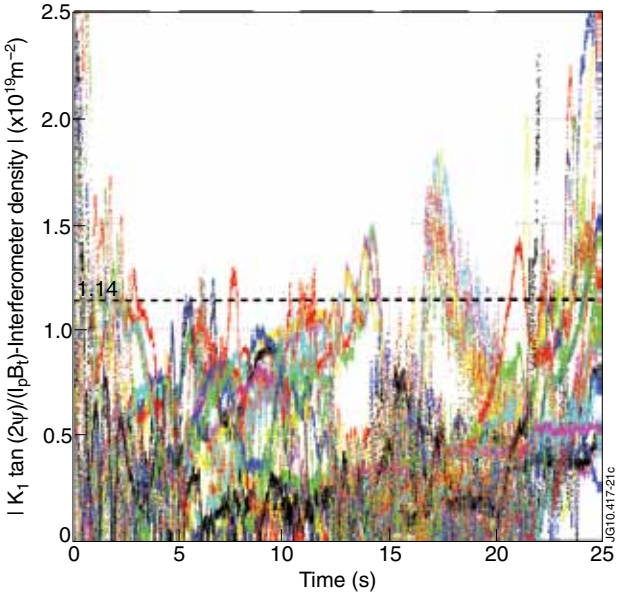

Figure 26: Statistical comparison of the interferometric density and the density calculated on the basis of equation (36).

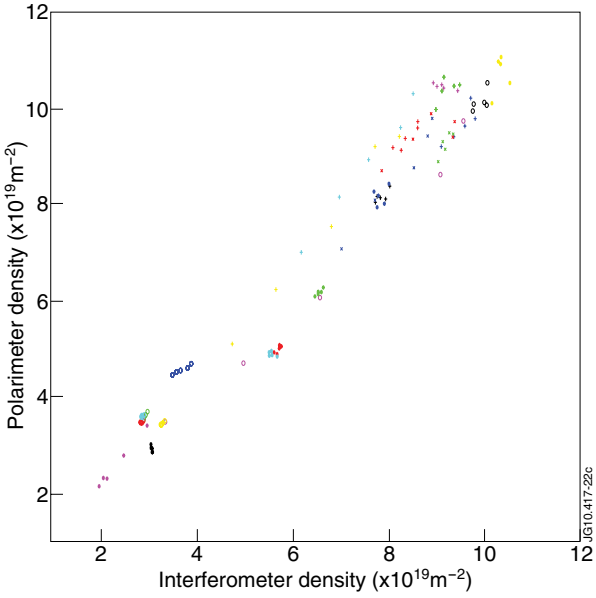

Figure 27: Polarimetric density estimated with equation (36) versus the interferometric measurement.

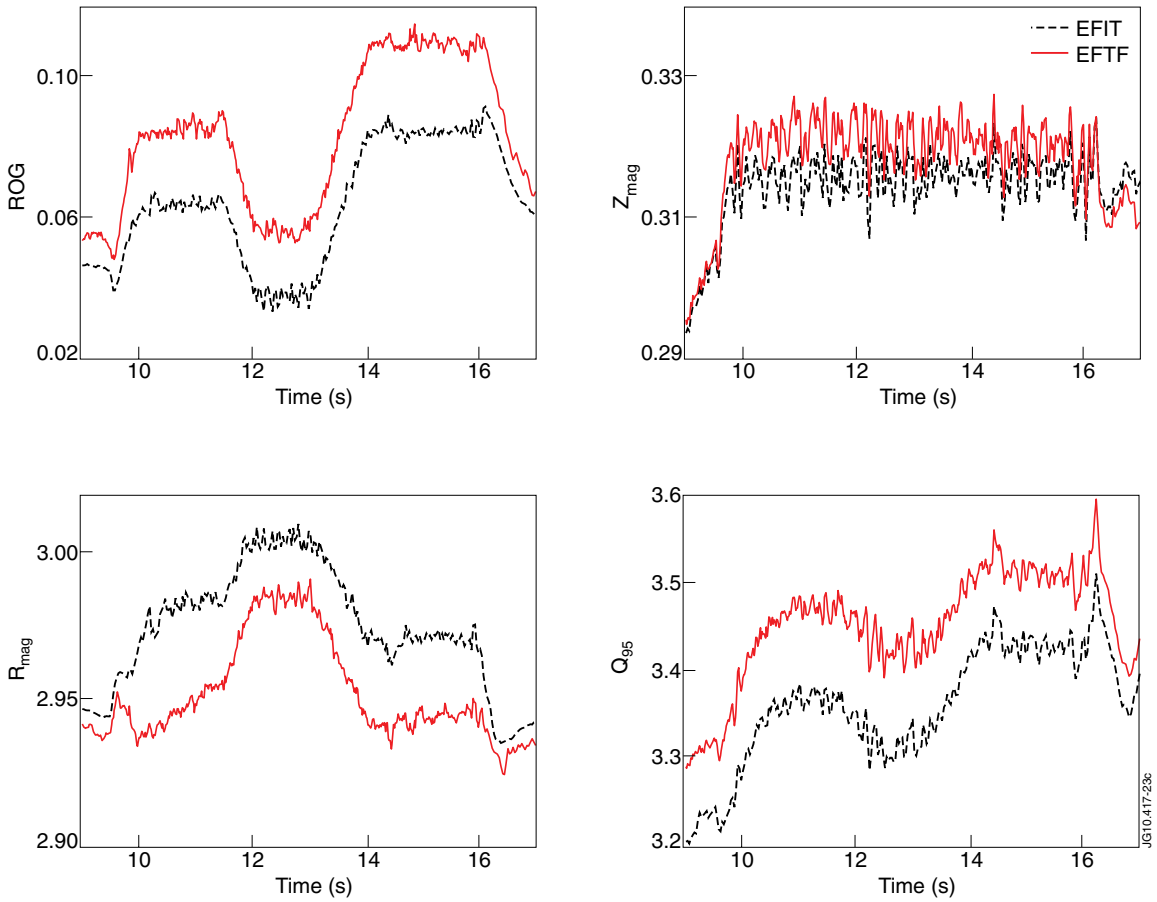

Figure 28: Comparison of the plasma geometrical parameters and the edge safety factor obtained with EFIT (blue line) and with EFTF (red line) for Pulse No: 77566. Z_{mag} is the vertical coordinate of the magnetic axis, R_{mag} the horizontal coordinate of the magnetic axis, ROG the plasma wall distance in the outer equatorial plane and q_{95} the safety factor at 95% of the plasma radius

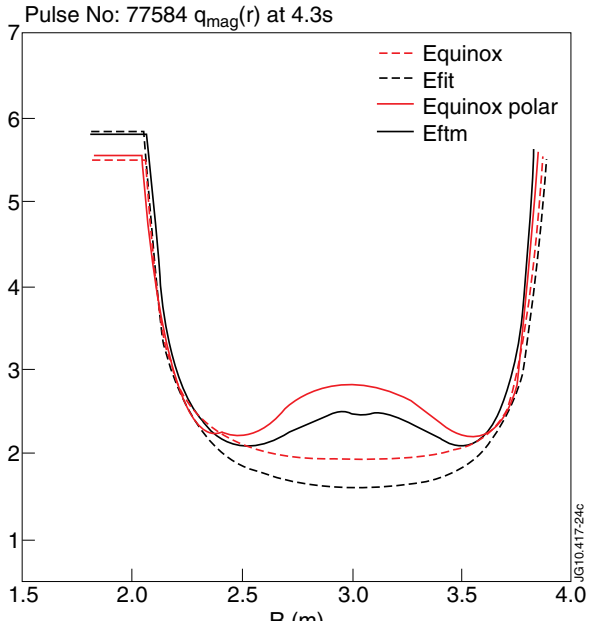

Figure 29: Comparison of the q profile generated by EQUINOX and EFIT with and without the polarimetric measurements. The dashed curves are the ones obtained without the polarimetric measurements and the continuous ones have been obtained with the polarimetric measurements.